SCIENTIFIC REPORTS

OPEN

SUBJECT AREAS:
NANOPARTICLES
BIOSENSORS

Received
19 August 2014

Accepted
2 October 2014

Published
22 October 2014

Correspondence and requests for materials should be addressed to J.H.Z. (jhzhan@sdu.edu.cn)

* These authors contributed equally to this work.

Tunable SERS-Tags-Hidden Gold Nanorattles for Theranosis of Cancer Cells with Single Laser Beam

Zhaolong Chen[1]*, Dexin Yu[1,2]*, Yu Huang[3], Zhengjun Zhang[3], Ting Liu[2] & Jinhua Zhan[1]

[1]Key Laboratory of Colloid and Interface Chemistry, Ministry of Education, Department of Chemistry, Shandong University, Jinan, Shandong, China, [2]Qilu Hospital of Shandong University, Jinan, Shandong, China, [3]Department of Materials Science and Engineering, Advanced Materials Laboratory, Tsinghua University, Beijing, China.

With the use of gold nanostructures, photothermal therapy (PTT) of cancer has great advantages compared to conventional methods, such as noninvasive targeted destruction and easily operation. Generally speaking, respective diagnosis and therapy of tumor require at least two instruments, leading to incongruence of tumor borders between diagnosis and therapy. To tackle this problem, tunable SERS-tags-hidden gold nanorattles (STHGNRs) have been designed and developed here for theranosis of cancer with single laser beam. The surface plasma resonance peak of STHGNRs can be tuned from visible region to near-infrared region by controlling the cavity size and shell thickness. The outer shells not only improve the stability of the SERS reporters but also enhance the brightness by more than two order magnitude compared to gold nanoparticles. In vitro study, immuno STHGNRs can serve as theranosis agents simultaneously for sensitive and efficient theranosis of cancer cells.

Cancer is one of the major causes of mortality all over the world[1]. Patients with cancer have been treated by numerous therapeutic methods including surgical extirpation, chemotherapy and radiation therapy[2–4]. Chemotherapy and radiation therapies have severe side effects and may cause substantial damage to healthy tissues and organs[2–5]. Surgical operation is limited to tumors that can be surgically observable and accessible, which also requires a comparatively long recovery time[6]. Photothermal therapy (PTT) as a minimally invasive treatment methodology has attracted much attention[7,8]. In PTT, the energy of optical radiation is absorbed and transformed into heat, causing denaturation of proteins and coagulation of tissue, which consequently cause irreversible damage to cells[9].

The absorption of optical radiation for heat conversion can be significantly enhanced by gold nanostructures, owing to their strong surface plasmon absorption[10,11]. Surface plasma resonance (SPR) peak of gold nanostructures depending on morphology and size can be easily tuned from visible region to near-infrared region (NIR) where blood and soft tissues are relatively transparent[12]. In recent years, various novel gold nanostructures with SPR peak in the NIR, such as gold nanorods[13–16], nanoshells[17–20] and nanocages[11,21–23] have been developed. Moreover, gold nanostructures have wonderful biocompatibility and chemical properties, suggesting their potential applications as photothermal therapeutic agents[24,25]. Immuno gold nanostructures can target to cancer cells selectively and ruin the cells effectively after irradiation.

Cancer therapies are still daunting owing to incongruence of tumor borders between diagnosis and therapy[26,27]. Generally, respective diagnosis and therapy of tumor require at least two instruments[28–30]. Fortunately, gold nanostructures are widely used as Surface Enhanced Raman scattering (SERS) substrates to enhance the Raman scattering efficiencies of adsorbed molecules by many orders of magnitude also due to its SPR properties[31–37]. Moreover, SERS has great prospect in biomedical diagnosis without suffering from rapid photobleaching, autofluorescence of biological samples and SERS tags are easily synthesized, cost effective and high sensitivity[31,32,34].

Here, we designed and developed tunable SERS-tags-hidden gold nanorattles (STHGNRs) for theranosis of cancer cells with single laser beam. In this design, SERS probes were adsorbed on the surface of the inner Au cores that are encapsulated in highly-crystalline Au outer shells. The outer nanoshells not only improve the stability of the SERS reporters but also enhanced the brightness of SERS reporters by more than two order magnitude compared to gold nanoparticles. In vitro studies, we have demonstrated that immuno STHGNRs can serve as theranosis agents simultaneously for sensitive and efficient theranosis of cancer cells.

Results

The realization of STHGNRs. The STHGNRs we developed for theranosis of cancer cells with single laser beam are schematically shown in Fig. 1a,which is based on the earlier publication[38]. Firstly, 13 nm diameter gold nanoparticles (GNPs, Fig. 1b) which serve as inner core were synthesized, followed by the exchange of the capping agent with a Raman reporter, namely, 6-Mercaptonicotinic acid (MNA). Then gold-MNA@silver sandwich nanostructures (GMSSNs) were synthesized by adding silver salt ($AgNO_3$) with a capping agent (CTAB) and a mild reducing agent (ascorbic acid). The VIS-NIR absorption spectrum (Fig. 1 d, red) shows the SPR peak of GMSSNs at around 480 nm, which is obviously different from the sharp plasmon absorption of solid silver nanoparticles. Finally, Ag shell of GMSSNs is replaced with gold by adding chloroauric acid ($HAuCl_4$). Au atoms epitaxially nucleate, grow into small island, and eventually evolve into a thin shell around each templates[39]. The products are hollow structures with inner core, called STHGNRs (Fig. 1 d). The SPR peak of STHGNRs (Fig. 1 d, blue) can be tuned to NIR. Fig. S1 shows the selected-area electron diffraction (SAED) pattern obtained from out shell of STHGNRs. These diffraction spots could be indexed to face center-cubic gold with a lattice constant of 4.08 Å, indicating the formation of a highly crystalline structure for the metallic wall. High resolution TEM (HRTEM) of outer shell in Fig. 1d shows resolved fringes separated by 2.45 and 1.96 Å, corresponding to the {111} and

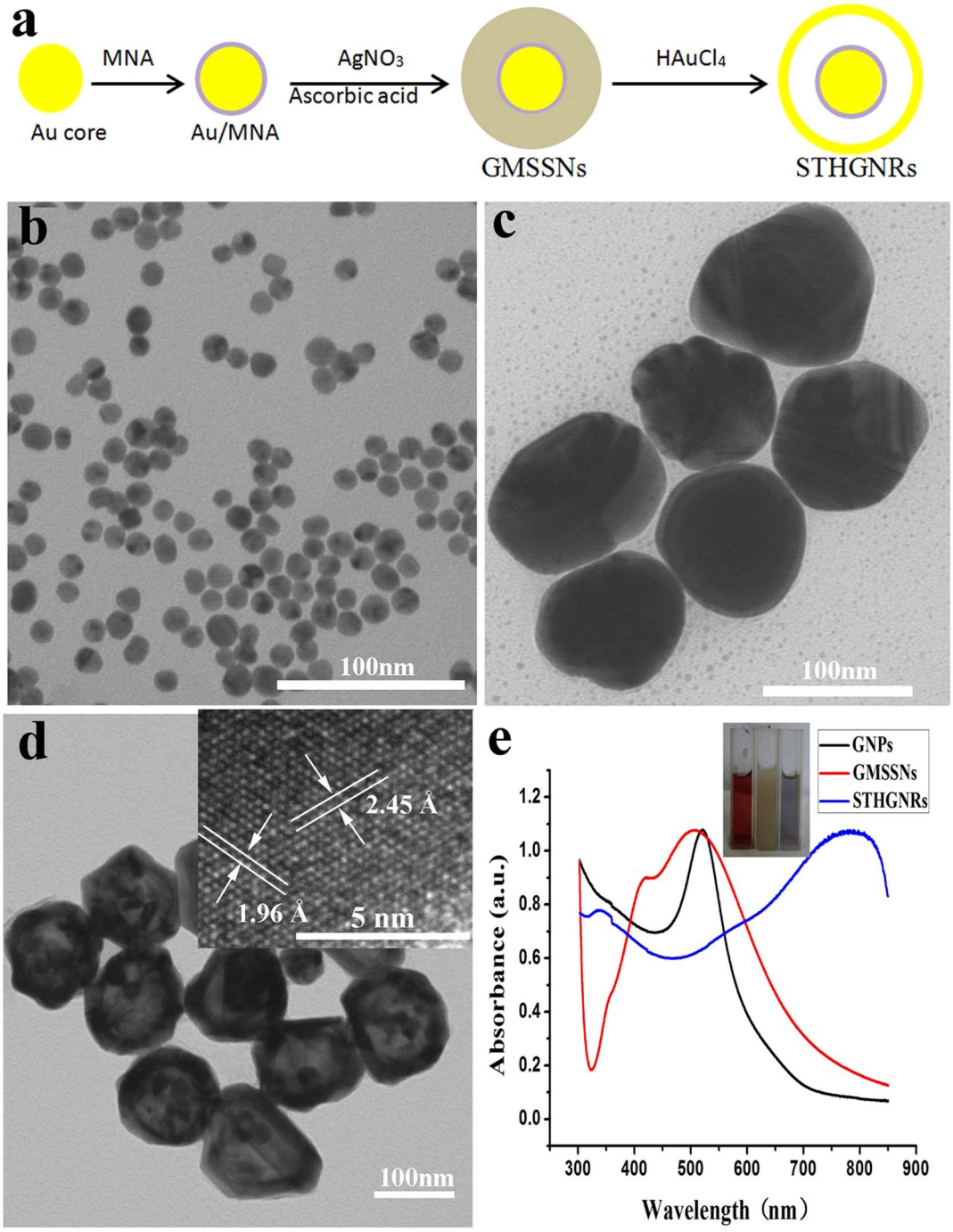

Figure 1 | The synthesis of STHGNRs. (a) Schematic illustration of design and synthesis of STHGNRs. (b) TEM image of GNPs employed as inner cores for the synthesis of STHGNRs. (c) TEM images of GMSSNs. (d) TEM images of STHGNRs and HRTEM of outer shell. (e) Vis-NIR absorption spectrum of GNPs, GMSSNs, STHGNRs and photograph of GNPs (claret), GMSSNs(yellow), STHGNRs(blue).

{200} lattice spacing of face-center cubic gold respectively. The inset in Fig. 1e is a photograph of these three nanostructures dispersion.

Tunable optical properties of STHGNRs. Optical properties of STHGNRs can be tuned by control the shell edge length and thickness. Fig. 2a indicates the SPR peak of STHGNRs conveniently tuned over a broad spectral range spanning from the visible region to the NIR by adding different volume 1 mM $HAuCl_4$ aqueous solution to 10 ml GMSSNs suspension. The progress of reaction can be easily monitored through its color changes. Fig. 2b shows Vis-NIR spectra of four samples of STHGNRs with different void size and shell thickness by control the Ag shell thickness of GMSSN. Note that sample 1, 2, 3, 4 are corresponding to the STHGNRs shown in Fig. S2a, b, c, d respectively. STHGNRs with absorption peak around 765 nm wavelength, targeted edge length around 133 nm and shell thickness around 13 nm were synthesized by a galvanic replacement reaction between GMSSNs (around 120 nm edge length, serving as sacrificial templates) and $HAuCl_4$.

The effects of shell edge length and thickness on optical properties of STHGNRs were further theoretically investigated in detail. Fig. S3 shows extinction spectra calculated of three STHGNRs models by applying the finite element method (FEM)[40,41]. The geometric parameters of three models respectively are: (a) 13 nm inner core, 133 nm edge length, 12 nm shell thickness; (b) 13 nm inner core, 140 nm edge length, 12 nm shell thickness; (c) 13 nm inner core, 133 nm edge length, 13 nm shell thickness. The dielectric functions of gold were modeled by the Lorentz-Drude dispersion model which was a smooth fit to the experimental optical constants[42]. And the STHGNRs were supposed to be full of water with the refractive index to be 4/3. Comparing model(a)with(b), the extinction peak would red-shift from 795 nm to 815 nm with increasing the edge length. Comparing model(b)with(c), the extinction peak is blue-shifted from 795 nm to 780 nm as the shell thickness is increased from 12 nm to 13 nm. Little discrepancy in the SPR peak and peak width was observed by comparing the calculated curve with Vis-NIR absorption spectra, owing to the distribution of edge length and shell thickness in real sample. Theoretical results also indicated that the SPR peak of STHGNRs can be tuned to NIR by controlling the size and shell thickness to enhance their potential in biomedical application.

The SERS enhancement of STHGNRs. Raman spectra were measured from colloidal samples of GNPs-MNA, GMSSNs and STHGNRs (Fig. 3a). Weak MNA Raman signal was observed from Au-MNA nanoparticles. As shown in methods, 0.5 ml Au-MNA nanoparticles were transformed into 65 ml GMSSNs and 70 ml STHGNRs. GMSSNs and STHGNRs exhibited clear, strong Raman signal of MNA. The SERS enhancement factor (EF) from GNPs in GMSSNs and STHGNRs was 4.88×10^2 times and 3.67×10^2 times higher than that from GNPs without out shell respectively. This result also indicates that Raman reporter molecules are hidden in GMSSNs because it has been known that large silver nanoparticles (>70 nm) were not optimal for SERS enhancement[43,44]. The remarkable EF factor of STHGNRs illuminates that STHGNRs can be utilized as an effective SERS tags.

The experimental results were theoretically analyzed. FEM calculations were performed to evaluate the local EM fields. For the FEM calculation, the diameter of GNPs model is 13 nm, the STHGNRs model with geometric parameters: 13 nm inner core, 133 nm edge length, 13 nm shell thickness were calculated. Fig. 3b shows the logarithmic distribution of local electric field $|E_{loc}/E_0|^4$ (i.e. the electromagnetic enhancement factor) of GNPs and STHGNRs at the excitation wavelength of 785 nm. For comparison, the relative intensity is plotted on the same color scale. Maximum value of GNPs logarithmic $|E_{loc}/E_0|^4$ is 2.26 while STHGNRs is 4.13. A much higher electric field is induced on the surface of inner core in STHGNRs compared with GNPs, giving so-called SERS "hot spots" in-built. Our theoretical result clearly suggests that GNPs served as inner core of STHGNRs can provide the most electromagnetic enhancement for SERS, which consistent with the experimental results well. Fig. S4b shows the slice $|E_{loc}/E_0|^4$ distribution of STHGNRs excited by 532 nm incident beam. We could notice the relative intensity of inner core was much lower than that excited by 785 nm beam.

Biofunctionalization and internalization of STHGNRs. The preparation of immuno STHGNRs was schematically illustrated as Fig. 4a shown. Firstly the surface of STHGNRs was modified with a mixture of thiol-PEG (~85%) and a heterofunctional PEG (SH-PEG-COOH) (~15%). Then, heterofunctional PEG was covalently conjugated to estrogen receptor-alpha antibody (ERa) that targets estrogen receptor (ER) which was over-expressed on a breast cancer cell (MCF-7) surface[45]. VIS-NIR absorption spectrum revealed a red-shift (~20 nm) in the SPR position after immunization (Fig. S5a). Hydrodynamic light scattering (DLS) data indicated the STHGNRs'

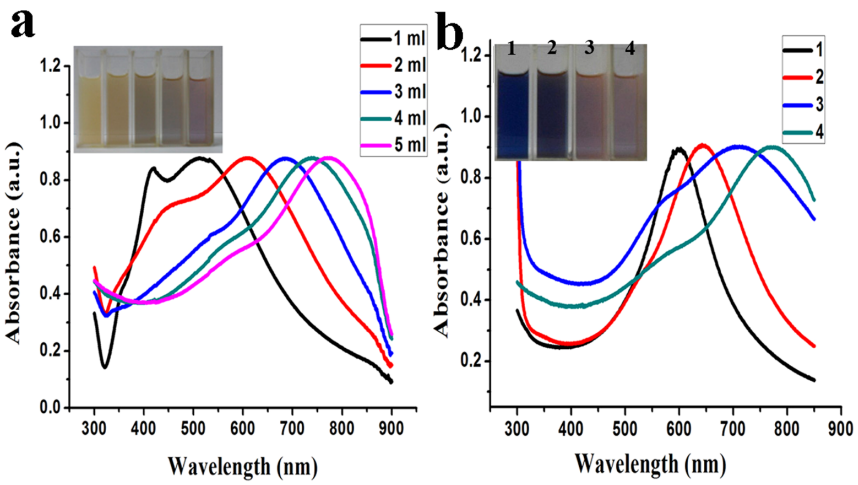

Figure 2 | Vis-NIR absorption spectra of STHGNRs. (a) Normalized Vis-NIR absorption spectra recorded from aqueous suspensions of nanostructures after titrating GMSSNs with different volume of a HAuCl4 aqueous solution and photograph of these nanostructures aqueous suspensions(from left to right are corresponding to 1, 2, 3, 4, 5 ml respectively). (b) Normalized Vis-NIR spectra recorded from the STHGNRs suspensions of different edge length and shell thickness. Note that sample 1, 2, 3, 4 are corresponding to the STHGNRs shown in Fig. S2a, b, c, d respectively and their SPR peak is tunable throughout the visible and near infrared regions by varying shell thickness and edge length.

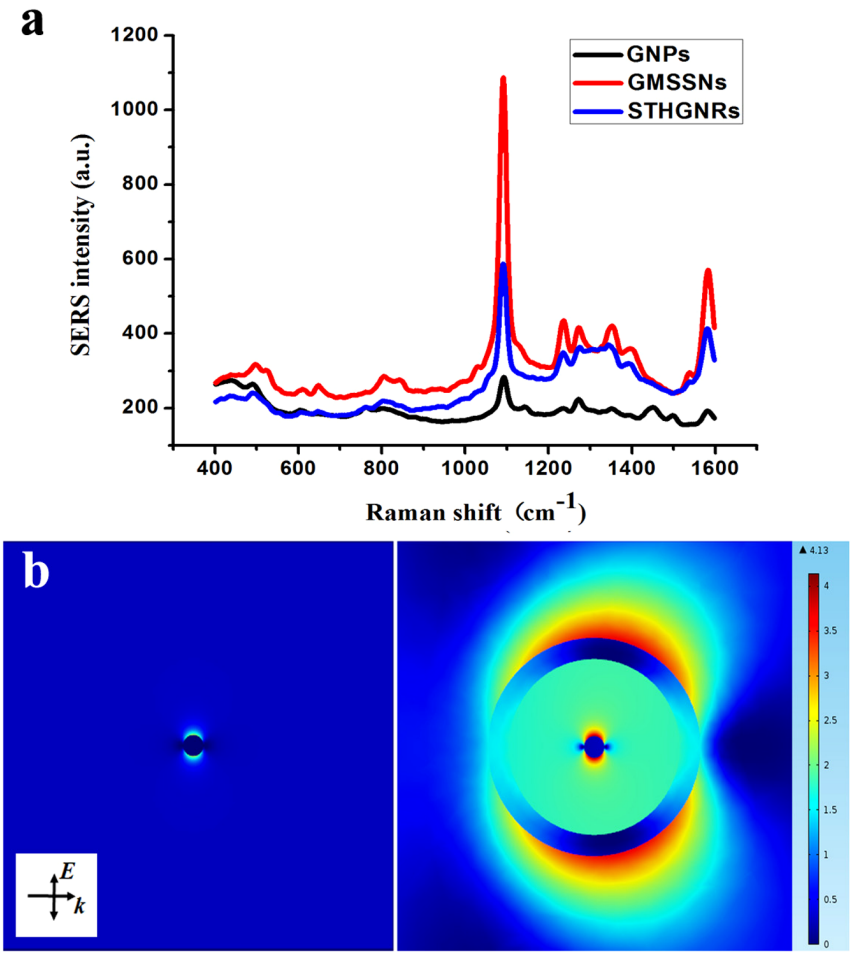

Figure 3 | The enhancement of GNPs and STHGNRs. (a) SERS spectra of Au-MNA nanoparticles and STHGNRs aqueous dispersion and note that 0.5 ml Au-MNA nanoparticles were transformed into 70 ml STHGNRs. (b) Slice logarithmic distribution of the local electric field $|E_{loc}/E_0|^4$ (EF) of different nanostructures at the excitation laser line of 785 nm: 13 nm GNPs; STHGNRs with geometric parameters: 13 nm inner core, 133 nm edge length, 13 nm shell thickness.

'wet' hydrodynamic diameter increased by nearly 60 nm owing to ERa conjugated to STHGNRs successfully (Fig. S5b,c). The stability of immuno STHGNRs in complex physiological fluid is critical and can be easily detected by SPR spectroscopy[32]. Only a small variation (<7 nm) in the SPR peak position was found over the four-day of incubation of immuno STHGNRs in 10% fetal bovine serum (FBS) by comparing VIS-NIR absorption spectra(Figure S6a), which indicates immuno STHGNRs is long term stable in physiological fluid. Figure S6b shows the SERS signals when the particles are stored in the same physiological fluids for several days, indicating that the SERS signals of Raman reporter molecules is high stable. The actively targeted STHGNRs were observed in cytosol from TEM imaging of ultrathin MCF-7 cell sections, revealing that some of the

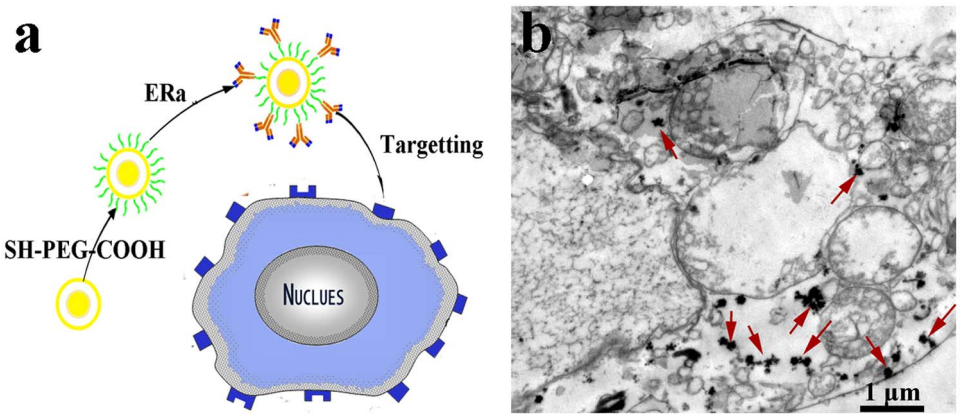

Figure 4 | Biofunctionalization and internalization of STHGNRs. (a) Schematic illustration of the biofunctionalization STHGNRs. (b) TEM image of sectioned actively-targeted MCF-7 cells showing the cancer cell uptake of biofunctionalized STHGNRs, their clustering and localization in intracellular organelles such as endosomes and cytoplasm.

nanostructures have been internalized possibly through endocytosis within three hours incubation period (Figure 4b).

Theranosis of cancer cell with single laser beam. STHGNRs with such intense Raman enhancement and tunable SPR features are ideal for SERS-guided PTT. Cancer cell SERS detection and PTT ability of STHGNRs with single laser were demonstrated in vitro study. A cell assay using MCF-7 cells was conducted to explore the SERS detection ability of STHGNRs, and all spectra were taken in cell suspensions. Fig. 5a, SERS signals that acquired from cancer cells incubated with immuno STHGNRs were reproducible and strong. For control, cells incubated with PEGylated STHGNRs shown a weak but reproducible signal of MNA. This low signals was probably caused by nonspecific binding and internalization of PEGylated STHGNRs or little PEGylated STHGNRs were not completely removed during cell isolation. No SERS signals of MNA were detected from cells incubated PBS suspension. These results illuminated that immuno STHGNRs can effective targeted to cancer cell and lead high concentration in cancer cells, which is significant for SERS detection and PTT.

To explore the PTT ability of immuno STHGNRs, MCF-7 cells in 96-well plates were incubated with immuno STHGNRs and PEGylated STHGNRs respectively for three hours. After removing the unbounded STHGNRs suspension and three rounds of washing, these cells were irradiated at a 785 nm laser power density of 5.24 W/cm^2 for 5 min. After irradiation, the cells were returned to a 37°C incubator for 1 h before the percentage of cellular viability was quantified by using 3-(4,5-dimethylthiazol-2-yl)-2,5-diphenyltetrazolium bromide (MTT) assay. It is clear that cells incubated with immuno STHGNRs exhibited more cellular damage than those incubated with PEGylated STHGNRs after irradiation. However, laser irradiation or immuno STHGNRs alone did not have significant effect on cellular viability under the same condition. It has been demonstrated that cellular membrane is broken after PTT[46]. Though a small experimental error was unavoidable during performing these treatments, the results clearly indicated that the immuno STHGNRs are effective to target cancer cells and absorb near-infrared light and convert it into heat for PTT.

Discussion

In this study, STHGNRs for theranosis of cancer cells were produced by a galvanic replacement reaction between GMSSNs and $HAuCl_4$. Their observed red-shift of SPR peak with increase of $HAuCl_4$ is mainly due to reduction of the shell thickness (Figure 2a), which is consistent with our theoretical analysis (Figure S3). On one hand, increasing void size while fixing the inner core size and shell thickness constant, will contribute to the absorption band red-shift as the plasmon oscillation decreases in energy. This result is consist with the optical properties of hollow gold nanospheres[47]. On the other hand, increasing shell thickness while fixing the inner core size and void size constant, will contribute to the SPR peak blue-shift. This result implies that STHGNRs takes on more solid-particle-like properties as inner cavity decreases and shell thickness increases. The SPR peak of 13 nm GNPs is approximately 520 nm. When it was trapped in hollow gold shell, the SPR peak would shift to lower energy, which can be explained with Halas' Plasmon Hybridization Theory[48]. The SPR peak of STHGNRs was readily tuned to NIR required for PTT and SERS detection by controlling the inner void sizes and shell thicknesses.

At present, SERS based biodetection remains in infancy owing to Raman reporters adhered to the surface of nanostructures produce relatively weak Raman signals and endure poor stability owing to enzymatic degradation or desorption of the Raman reporters in physiological environment[32,49]. Here, Raman reporter molecules are absorbed on the surface of the inner Au cores that are encapsulated in highly-crystalline Au outer shells. The outer nanoshells not only protect Raman reporter molecules from enzymatic degradation during cancer detection and treatment, but also offer in-built EM hot-spots. The SERS enhancement factor (EF)calculated from GNPs served as inner core of STHGNRs was over two orders of magnitude higher than that from GNPs (Figure 3). Theoretical calculation results confirm that GNPs in STHGNRs have much higher electric-field intensity enhancement than that without shell at 785 nm excitation, which aligned well with our experimental results. Conventional SERS tags with Raman reporters absorbed on the surface of nanostructures depend on random clustering of nanostructures to produce EM hot-spots, which is totally in contrast to our design suggested here. The high stability and enhancement of SERS probe molecules is essential for SERS detection in complex physiological environment. Moreover, STHGNRs with SPR peak in the NIR has much higher electric-field intensity under 785 nm excitation than 532 nm excitation as shown in Fig. S3. This result

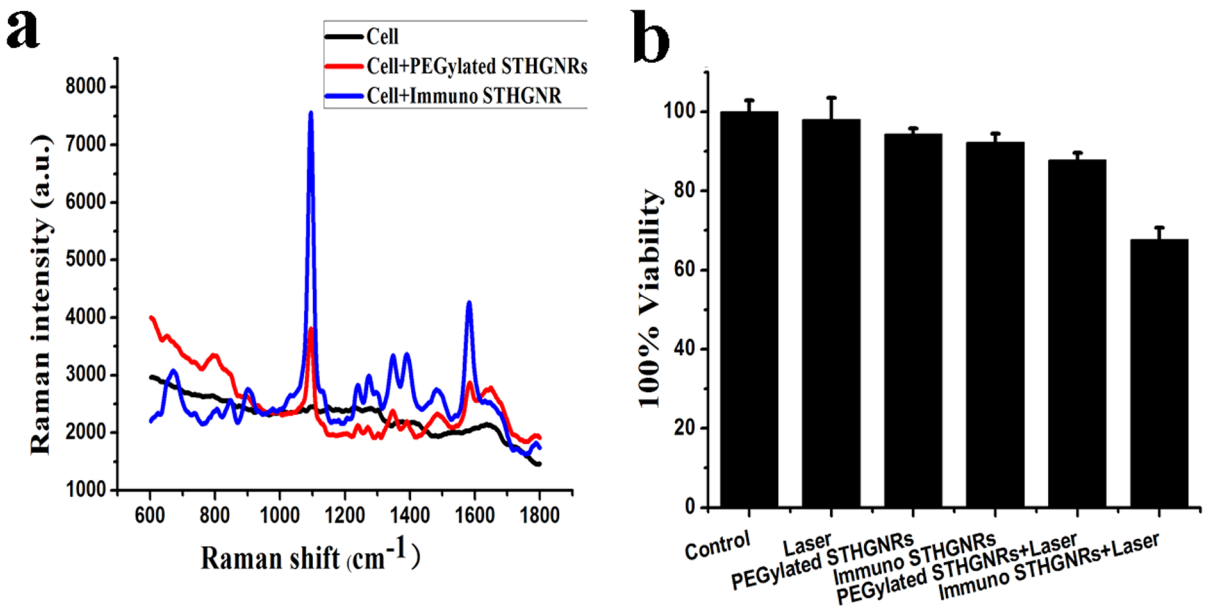

Figure 5 | SERS detection and PTT of cancer cell. (a) SERS signals from cell suspensions incubated with immuno STHGNRs (red), PEGylated STHGNRs(black) and PBS (blue). (b) MTT assay revealing the cell viability after MCF-7 cells incubating with PBS, PEGylated STHGNRs, immuno STHGNRs and PTT.

implies that STHGNRs can be used in biomedical detection with high sensitivity under NIR beam, which is consistent with the requirement of PTT.

The ability of STHGNRs for theranosis of cancer cells with single laser beam was also demonstrated in vitro study. ERa was used to specifically recognize the ER on the MCF-7 cells surface. The first type of control experiment was conducted by incubating cells with PBS and irradiation. No SERS signals of MNA and cellular damage were observed (Fig. 5a,b). In the second control experiment, cells were incubated with PEGylated STHGNRs and irradiated with laser beam. Only weak fingerprint spectral signature of MNA and little cellar damage were observed, indicating nonspecific binding of PEGylated STHGNRs. In the third type of control experiment, cells incubated with immuno STHGNRs and then suffered from irradiation. More intense and reproducible SERS signals of MNA and much greater cellular damage were observed compared to the second control group. Thus, it can be concluded that immuno STHGNRs is able to target to cancer cells effectively and improve the effect of detection and destruction of cancer cells simultaneously.

In summary, we demonstrate a simple, yet powerful SERS-guided PTT agent design of STHGNRs in which Raman reporters are absorbed on the surface of the inner Au cores that are encapsulated in highly-crystalline Au outer shells. The outer nanoshells not only protect Raman reporter molecules from enzymatic degradation during cancer detection and treatment, but also enhance the Raman intensity of Raman reporter molecules by more than two order magnitude due to the coupling of near field electromagnetic fields of the inner Au cores and the outer Au shells. Moreover, SPR peak of STHGNRs can be tuned from visible region to NIR by controlling the shell thickness and edge length. In vitro study, we demonstrated that immuno STHGNRs are very effective for photothermal ruin of cancer cells and are very sensitive for SERS detection with single laser beam. It is expected to enable high resolution, non-invasive Raman-based detection, and targeted, effective cellular damage, which may open up new possibilities in image-guided therapy with single laser beam.

Methods

Reagent. Gold (III) chloride trihydrate ($HAuCl_4 \cdot 3H_2O$), Trisodium citrate dihydrate ($Na_3Ct \cdot 2H_2O$), Hexadecyltrimethylammonium bromide (CTAB), Ascorbic acid (AA), silver nitrate($AgNO_3$), Disodium hydrogen phosphate(Na_2HPO_4), Potassium dihydrogen phosphate (KH_2PO_4), Potassium chloride (KCl), Hexadecyltrimethylammonium bromide (CTAB) and sodium hydroxide (NaOH) were all purchased from Sinopharm Chemical Reagent CO., Ltd. (Shanghai, China). N-(3-dimethylaminopropyl)-N-ethylcarbodiimidehydrochloride (EDC) and N-hydroxy succinimide (NHS) were purchased from Aladdin Chemistry CO., Ltd. 6-Mercaptonicatinic acid (MNA) was purchased from Sigma-aldrich. (Shanghai, China).SH-mPEG(Mw = 5000 Da) and SH-PEG-COOH(Mw = 5000 Da) were obtained from Xibao Medpep Co., Ltd. (Shanghai, China).Estrogen Receptor-alpha Antibody was purchased from EnoGene Biotech Co.,Ltd. 1640 Culture medium and fetal bovine serum(FBS) was purchased from Gibco Co., Ltd. Pancreatic enzymes was purchased from abcam Co.,Ltd. MCF-7 cell line was purchased from Shanghai Bioleaf Biotech Co.,Ltd. Ultra-pure water (18.25 MΩ·cm) was used throughout the experiment. Phosphate buffered solution (PBS) (pH 7.4, 0.1 M) was prepared with 0.1 M Na_2HPO_4, 0.1 M KH_2PO_4 and 0.1 M KCl and used as working buffer solution.

Preparation of gold nanoparticles. 13 nm gold nanoparticles were prepared as reported[50]. Typically, 2 ml 1% $HAuCl_4$ aqueous solution was mixed with 100 ml ultrapure water in a 250 ml flask, and then heated to boiling under violent stir. After 10 mins, 4 ml 2.3% Na_3Ct aqueous solution was injected quickly and remain boiling for 30 mins, claret colloid which surface plasmon peak at 520 nm was obtained.

Preparation of the GMSSNs. 20 ul MNA alcohol solution (1 mM) as a Raman-active probes were added to 1 ml of the gold colloid, and reacted for one night. MNA molecules were conjugated to GNPs via -SH terminal groups. Then the MNA modified gold nanoparticles were centrifuged at 10000 rpm, for 8 mins, and rinsed with ultrapure water twice in order to remove the unreacted MNA. For coating gold nanoparticles with a layer of silver, typically, 0.9112 g CTAB were dissolved in 50 ml ultrapure water and heated to 60°C in oil bath under stirring. Then 5 mL 0.1 M AA, 10 mL 10 mM $AgNO_3$ solutions and 0.5 mL MNA modified Au colloid were injected to the reaction system. Shortly after injecting gold colloid, 0.6 mL of 1.0 M NaOH was added dropwise. Then the color of reaction system change from claret into yellow-brown.

Transfer GMSSNs into STHGNRs. In a typical synthesis, transfer 10.0 mL of this sandwich solution to a 50 mL flask under magnetic stirring and then heated at 60°C for 10 min. A specific amount (as indicated in the text) of 1 mM $HAuCl_4$ aqueous solution was added into the flask through a syringe dropwise under magnetic stirring, and heated for another 5 min. Once cooled to room temperature, the sample was centrifuged and purified before use.

Preparation of immuno STHGNRs. The STHGNRs (4 nM, 1 mL) were incubated with 1 ml 4 mM an aqueous solution of the mixture of thiol-PEG (~85%) and a heterofunctional PEG (SH-PEG-COOH) (~15%) at room temperature in the dark for 12 h. The reaction mixture was centrifuged to remove the byproducts and unreacted PEG. After washed with water twice, the sample redispersed in PBS. Then EDC solution (5 ul, 40 mg/ml) and sulfo-NHS (5 ul, 110 mg/ml) were added to PEGylated STHGNRs suspension at 25°C for 15 min to active –COOH groups. To target MCF-7 cells, the actived PEGylated STHGNRs mixed with monoclonal ERa in PBS overnight at 4°C. The sample was centrifuged for 5 min at 10 000 rpm to remove unreacted antibodies and redispersed in 1 mL of PBS and stored at 4°C .

Cell Culture. The breast cancer cell line MCF-7 was cultured in 1640 medium modified containing 10% FBS and 5% streptomycin/penicillin at 37°C in 5% CO_2. The medium was changed 2–3 times a week. When they reached a confluency of 60–90%, the adherent cells were removed from the growth vessel with trypsin. The trypsin was deactivated by adding the growth medium. The suspension of cells was centrifuged for 5 min at 1000 rpm, and the pellet of cells was resuspended in growth medium and then transferred to a desired growth plate for SERS detection and photothermal studies.

Cellular SERS studies. MCF-7 cell in 12-well plates were incubated with 200 uL 2 nM of the immuno GYSNs or PEGylated STHGNRs for 3 h. The STHGNRs suspensions were removed and rinsed with PBS for three times. The adherent cells were removed from the well with trypsin and centrifuged for 5 min at 1000 rpm, washed with PBS for twice. The cells were resuspended in 500 ul PBS with a cell density of 1.5×10^6 cells per ml and transferred into a quartz cuvette to get the SERS spectrum. An additional portion of the cells received only PBS, and were used as controls to assess background cell scattering.

PTT of cancer cells. MCF-7 cells in 96-well plates were incubated with 20 uL of the immuno STHGNRs, PEGylated or PBS for 3 h. After removing the unbounded STHGNRs suspension, the cells rinsed with PBS for three times. The cells in the center of the wells were irradiated with a 785 nm laser, power density of 5.24 W/cm^2 for 5 mins. The spot size was 2.4 mm in diameter and only 12.6% of cell in each well were irradiated. Then, the cells were returned to a 37°C incubator for 1 h before the percentage of cellular viability was quantified by using MTT assay.

1. Altekruse, S. *et al.* SEER Cancer statistics review 1975–2007 (2010) 20/06/2012.
2. Sachdeva, M. S. Drug targeting systems for cancer chemotherapy. *Exp. Opin. Invest. Drugs* **7**, 1849–1864 (1998).
3. Torchilin, V. P. Drug targeting. *Eur. J. Pharm. Sci* **11**, S81–S91 (2000).
4. Partridge, A. H., Burstein, H. J. & Winer, E. P. Side effects of chemotherapy and combined chemohormonal therapy in women with early-stage breast cancer. *J. Natl. Cancer Inst. Monogr* **30**, 135–142 (2001).
5. Donaldson, S. S. Nutritional consequences of radiotherapy. *Cancer Res* **37**, 2407–2413 (1977).
6. Miller, A. B., Hoogstraten, B., Staquet, M. & Winkler, A. Reporting results of cancer treatment. *Cancer* **47**, 207–214. (1981).
7. Amin, Z. *et al.* Hepatic metastases: interstitial laser photocoagulation with real-time US monitoring and dynamic CT evaluation of treatment. *Radiology* **187**, 339–347 (1993).
8. Nolsøe, C. P. *et al.* Interstitial hyperthermia of colorectal liver metastases with a US-guided Nd-YAG laser with a diffuser tip: a pilot clinical study. *Radiology* **187**, 333–337 (1993).
9. Anderson, R. R. & Parrish, J. A. Selective photothermolysis: precise microsurgery by selective absorption of pulsed radiation. *Science* **220**, 524–527 (1983).
10. Pissuwan, D., Valenzuela, S. M. & Cortie, M. B. Therapeutic possibilities of plasmonically heated gold nanoparticles. *Trends Biotechnol* **24**, 62–67 (2006).
11. Chen, J. *et al.* Immuno gold nanocages with tailored optical properties for targeted photothermal destruction of cancer cells. *Nano Lett.* **7**, 1318–1322 (2007).
12. Weissleder, R. A clearer vision for in vivo imaging. *Nat. Biotechnol* **19**, 316–317 (2001).
13. Link, S. & El-Sayed, M. A. Spectral properties and relaxation dynamics of surface plasmon electronic oscillations in gold and silver nanodots and nanorods. *J. Phys. Chem. B* **103**, 8410–8426 (1999).
14. Murphy, C. J. *et al.* Anisotropic metal nanoparticles: synthesis, assembly, and optical applications. *J. Phys. Chem. B.* **109**, 13857–13870 (2005).
15. Kelly, K. L., Coronado, E., Zhao, L. L. & Schatz, G. C. The optical properties of metal nanoparticles: the influence of size, shape, and dielectric environment. *J. Phys. Chem. B.* **107**, 668–677 (2003).
16. von Maltzahn, G. *et al.* Computationally guided photothermal tumor therapy using long-circulating gold nanorod antennas. *Cancer Res* **69**, 3892–3900 (2009).
17. Oldenburg, S. J., Averitt, R. D., Westcott, S. L. & Halas, N. J. Nanoengineering of optical resonances. *Chem. Phys. Lett.* **28**, 243–247 (1998).

18. Averitt, R. D., Westcott, S. L. & Halas, N. J. Linear optical properties of gold nanoshells. *JOSA B* **16**, 1824–1832 (1999).
19. Hirsch, L. R. *et al.* Nanoshell-mediated near-infrared thermal therapy of tumors under magnetic resonance guidance. *Proc. Natl. Acad. Sci.* **100**, 13549–13554 (2003).
20. Liu, H. *et al.* Multifunctional gold nanoshells on silica nanorattles: a platform for the combination of photothermal therapy and chemotherapy with low systemic toxicity. *Angewandte Chemie* **50**, 891–895 (2011).
21. Sun, Y. & Xia, Y. Shape-controlled synthesis of gold and silver nanoparticles. *Science* **298**, 2176–2179 (2002).
22. Sun, Y. & Xia, Y. Mechanistic study on the replacement reaction between silver nanostructures and chloroauric acid in aqueous medium. *J. Am. Chem. Soc.* **126**, 3892–3901 (2004).
23. Yavuz, M. S. *et al.* Gold nanocages covered by smart polymers for controlled release with near-infrared light. *Nat. Mater.* **8**, 935–939 (2009).
24. Hu, M. *et al.* Gold nanostructures: engineering their plasmonic properties for biomedical applications. *Chem. Soc. Rev.* **35**, 1084–1094 (2006).
25. Xia, Y. & Halas, N. J. Shape-controlled synthesis and surface plasmonic properties of metallic nanostructures. *MRS Bull.* **30**, 338–343 (2005).
26. Reinges, M. H. T. *et al.* Course of brain shift during microsurgical resection of supratentorial cerebral lesions: limits of conventional neuronavigation. *Acta Neurochir. (Wien)* **146**, 369–377 (2004).
27. Luo, S. *et al.* A multifunctional heptamethine near-infrared dye for cancer theranosis. *Biomaterials* **34**, 2244–2251 (2013).
28. Gobin, A. M. *et al.* Near-infrared resonant nanoshells for combined optical imaging and photothermal cancer therapy. *Nano Lett.* **7**, 1929–1934 (2007).
29. Koo, H. *et al.* In vivo targeted delivery of nanoparticles for theranosis. *Acc. Chem. Res.* **44**, 1018–1028 (2011).
30. Gandra, N., Portz, C. & Singamaneni, S. Multifunctional plasmonic nanorattles for spectrum-guided locoregional therapy. *Adv. Mater.* **26**, 424–429 (2014).
31. Qian, X. *et al.* In vivo tumor targeting and spectroscopic detection with surface-enhanced Raman nanoparticle tags. *Nat. Biotechnol.* **26**, 83–90 (2008).
32. Gandra, N. & Singamaneni, S. Bilayered Raman-intense gold nanostructures with hidden tags (BRIGHTs) for high-resolution bioimaging. *Adv. Mater.* **25**, 1022–1027 (2013).
33. Albrecht, M. G. & Creighton, J. A. Anomalously intense Raman spectra of pyridine at a silver electrode. *J. Am. Chem. Soc.* **99**, 5215–5217 (1977).
34. von Maltzahn, G. *et al.* SERS-coded gold nanorods as a multifunctional platform for densely multiplexed near-infrared imaging and photothermal heating. *Adv. Mater.* **21**, 3175–3180 (2009).
35. Cao, Y. C., Jin, R. & Mirkin, C. A. Nanoparticles with Raman spectroscopic fingerprints for DNA and RNA detection. *Science* **297**, 1536–1540 (2002).
36. Ni, J., Lipert, R. J., Dawson, G. B. & Porter, M. D. Immunoassay readout method using extrinsic Raman labels adsorbed on immunogold colloids. *Anal. Chem.* **71**, 4903–4908 (1999).
37. Lu, W. *et al.* Gold nano-popcorn-based targeted diagnosis, nanotherapy treatment, and in situ monitoring of photothermal therapy response of prostate cancer cells using surface-enhanced Raman spectroscopy. *J. Am. Chem. Soc.* **132**, 18103–18114 (2010).
38. Sun, Y. G., Wiley, B., Li, Z. Y. & Xia, Y. N. Synthesis and optical properties of nanorattles and multiple-walled nanoshells/nanotubes made of metal alloys. *J. Am. Chem. Soc.* **126**, 9399–9406 (2004).
39. Chen, J. *et al.* Gold nanocages: engineering their structure for biomedical applications. *Adv. Mater.* **17**, 2255–2261 (2005).
40. Zhao, J. *et al.* Methods for describing the electromagnetic properties of silver and gold nanoparticles. *Acc. Chem. Res.* **41**, 1710–1720 (2008).
41. Wustholz, K. L. *et al.* Structure-activity relationships in gold nanoparticle dimers and trimers for surface-enhanced Raman spectroscopy. *J. Am. Chem. Soc.* **132**, 10903–10910 (2010).
42. Rakic, A. D., Djurišic, A. B., Elazar, J. M. & Majewski, M. L. Optical properties of metallic films for vertical-cavity optoelectronic devices. *Appl. Opt.* **37**, 5271–5283 (1998).
43. Stamplecoskie, K. G., Scaiano, J. C., Tiwari, V. S. & Anis, H. Optimal size of silver nanoparticles for surface-enhanced Raman spectroscopy. *J. Phys.Chem. C* **115**, 1403–1409 (2011).
44. Feng, Y. *et al.* Engineering "hot" nanoparticles for surface-enhanced Raman scattering by embedding reporter molecules in metal layers. *Small* **8**, 246–251 (2011).
45. Pelekanou, V. *et al.* The estrogen receptor alpha-derived peptide ERalpha17p (P(295)-T(311)) exerts pro-apoptotic actions in breast cancer cells in vitro and in vivo, independently from their ERalpha status. *Mol. Oncol.* **5**, 36–47 (2011).
46. Au, L. *et al.* A quantitative study on the photothermal effect of immuno gold nanocages targeted to breast cancer cells. *Acs Nano* **2**, 1645–1652 (2008).
47. Schwartzberg, A. M., Olson, T. Y., Talley, C. E. & Zhang, J. Z. Synthesis, characterization, and tunable optical properties of hollow gold nanospheres. *J. Phys. Chem. B.* **110**, 19935–19944 (2006).
48. Halas, N. J., Lal, S., Chang, W. S., Link, S. & Nordlander, P. Plasmons in strongly coupled metallic nanostructures. *Chem. Rev.* **111**, 3913–3961 (2011).
49. Talley, C. E. *et al.* Surface-enhanced Raman scattering from individual Au nanoparticles and nanoparticle dimer substrates. *Nano Lett.* **5**, 1569–1574 (2005).
50. Ji, X. *et al.* Size control of gold nanocrystals in citrate reduction: the third role of citrate. *J. Am. Chem. Soc.* **129**, 13939–13948 (2007).

Acknowledgments

We thank the financial support from National Basic Research Program of China (973 Program 2013CB934301), National Natural Science Fund of China (NSFC 21377068 and 21075077), Shandong Provincial Natural Science Foundation for Distinguished Young Scholars (JQ201004) and Independent Innovation Foundation of Shandong University (IIFSDU-2012JC027) and Taishan college of Shandong university.

Author contributions

J.H.Z., Z.L.C. and D.X.Y. designed the project and experiments, and wrote the manuscript; Z.L.C. performed nanostructures design, synthesis and characterization; D.X.Y. and T.L. conducted cellar study; Y.H. and Z.J.Z. performed the computational analysis; J.H.Z. supervised the project.

Additional information

Supplementary information accompanies this paper at http://www.nature.com/scientificreports

Competing financial interests: The authors declare no competing financial interests.

How to cite this article: Chen, Z. *et al.* Tunable SERS-Tags-Hidden Gold Nanorattles for Theranosis of Cancer Cells with Single Laser Beam. *Sci. Rep.* **4**, 6709; DOI:10.1038/srep06709 (2014).